Three-dimensional hopping conduction triggered by magnetic ordering in the quasi-one-dimensional iron-ladder compounds $BaFe_2S_3$ and $BaFe_2Se_3$

Yuk Tai Chan,[1,*] Seulki Roh,[1] Soohyeon Shin,[2] Tuson Park,[2] Martin Dressel,[1] and Ece Uykur[1]

[1]*1. Physikalisches Institut, Universität Stuttgart, 70569 Stuttgart, Germany*

[2]*Center for Quantum Materials and Superconductivity (CQMS) and Department of Physics, Sungkyunkwan University, Suwon, 16419, Republic of Korea*

(Received 1 May 2020; accepted 29 June 2020; published 9 July 2020)

Because the iron-ladder compounds $BaFe_2X_3$ (X = S or Se) possess highly anisotropic crystal, electronic, and magnetic structures, the order in certain degrees of freedom leads to interesting interplays among them. Here we present a systematic study of the dielectric behavior of $BaFe_2S_3$ and $BaFe_2Se_3$ along all crystallographic directions revealing the conduction mechanism and its relation to the underlying magnetic ordering. The temperature dependence of the DC conductivity indicates that the antiferromagnetic order is accompanied by a transition in the conduction mechanism from a simple activated behavior above T_N to three-dimensional variable range hopping below T_N. Although the magnetic structures that develop on $BaFe_2S_3$ and $BaFe_2Se_3$ are rather different—despite nearly identical crystal structures—we do not find significant difference in the conduction mechanism.

DOI: 10.1103/PhysRevB.102.035120

I. INTRODUCTION

The interaction between magnetic and electronic orders often results in exotic phenomena such as quantum criticality, multiferroicity, possible superconductivity, and other broken symmetry ground states. In this context, materials with extraordinary magnetic structures are of interest in condensed matter science as they manifest peculiar physical behaviors. Among them $BaFe_2X_3$ (X = S or Se), with their unique iron-containing quasi-one-dimensional (1D) ladder structure, the remarkable magnetic ordering [1–3], and the emergence of superconductivity under pressure [4–7], constitutes a promising platform for detailed investigations. The discovery of superconductivity is particularly exciting because it is the first iron-based superconductor that consists of spin ladders, instead of a square lattice, resembling the situation in cuprates [5,8]. Thus, $BaFe_2X_3$ (X = S or Se) offers an unprecedented opportunity to bridge between the physics of iron-based and cuprate superconductors; it naturally deserves research attention on its own.

Often overshadowed by the superconducting phase that emerges under pressure, $BaFe_2X_3$ (X = S or Se) features rich physics at ambient pressure, as well. $BaFe_2S_3$ and $BaFe_2Se_3$ crystallize into two nearly identical phases, space group *Cmcm* for the former and *Pnma* for the latter compound [Figs. 1(a) and 1(b)], where the ladders in $BaFe_2Se_3$ are slightly tilted [2,9–11]. Both materials are insulators (or semiconductors) with narrow band gaps, where $\Delta \simeq 0.06$ and 0.13 eV for $BaFe_2S_3$ and $BaFe_2Se_3$, respectively [12,13]. With decreasing temperature, a gradual formation of antiferromagnetic (AFM) order occurs, where T_N depends on the growth conditions ranging from 85 to 120 K [5,14] for $BaFe_2S_3$ and from 160 to 230 K [14,15] for $BaFe_2Se_3$. The AFM ordering introduces different magnetic dipole configurations, stripe type (*CX* type) and block type in $BaFe_2S_3$ and $BaFe_2Se_3$, respectively [1,7,16].

Despite the various experimental efforts, important questions, such as the dimensionality of the electronic properties, remain unanswered. Given the prominent anisotropic lattice and magnetic structure, one expects the conduction to follow this anisotropy. While most transport measurements are confined to the leg direction [4–6,12,17–19], no consensus on the issue can be found in the scarce literature that examines different orientations [14,20,21]. Apart from the magnitude of the conductivity, the transport mechanism is also expected to be linked to the magnetic order and configuration in the AFM phase. In fact, arguments on the thermally activated conduction [14,19,22,23] or on the dimensionality of the conduction [10,13,17,18] have been frequently given from transport measurements. However, these efforts mainly focused on the leg direction and the discussions do not consider the existence of the strong AFM background. Therefore, a true understanding of the interplay between electronic and magnetic properties has not been achieved, yet.

On the other hand, the combination of block-type AFM and tilted ladder structure is expected to give rise to the multiferroic behavior in $BaFe_2Se_3$ [24]. The magnetic transition constructs the block-type spin arrangement which breaks the parity and space inversion symmetry for the neighboring selenium. Se atoms, above a block or within two blocks, are relocated differently, leading to an unequal spacial separation from the iron ladder for adjacent Se atoms. This results in a local electric polarization perpendicular to the ladder plane. Although the polarization is offset between ladder layers, a net microscopic polarization along rung direction might still be observable due to the tilted ladders. Indeed, a recent optical second-harmonic-generation experiment detects an electronic polar state accompanied by a structural transition above T_N

*yuk-tai.chan@pi1.uni-stuttgart.de

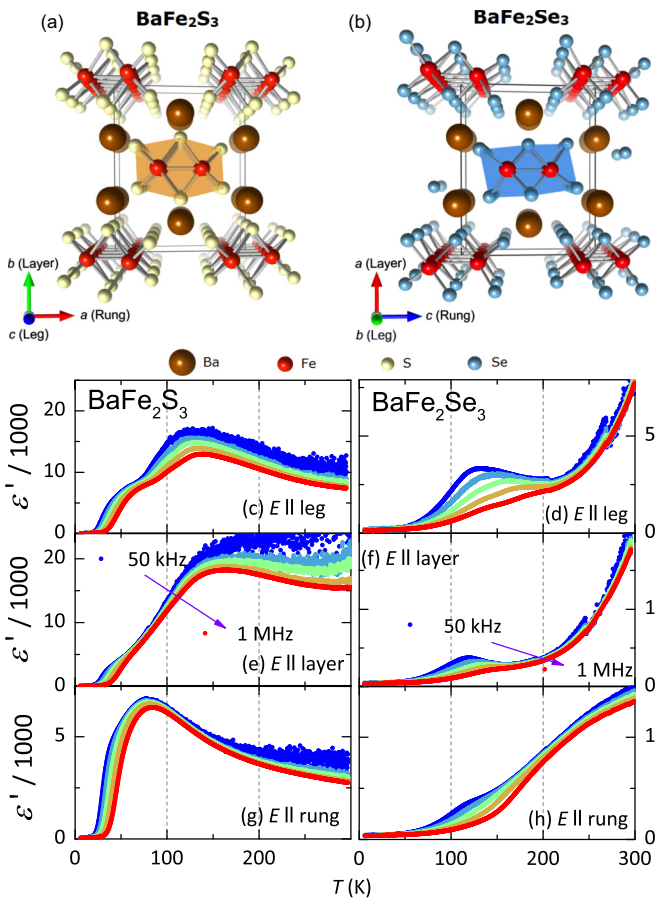

FIG. 1. (a) and (b) Crystal structures of $BaFe_2S_3$ and $BaFe_2Se_3$ by looking along the ladder direction. The rungs are directed horizontally. The ladders in $BaFe_2Se_3$ are slightly tilted compared to $BaFe_2S_3$. (c)–(h) Temperature-dependent real part of the dielectric permittivity measured along the leg, layer, and rung directions of $BaFe_2S_3$ (left) and $BaFe_2Se_3$ (right).

(at 400 K) [25], puzzling the relation between the observed electronic polar state and the magnetic one.

In order to answer the open questions posed above, here we report a systematic dielectric study on both $BaFe_2S_3$ and $BaFe_2Se_3$. Dielectric spectroscopy is a suitable tool for detecting the ferroelectric nature as the formation of ferroelectric ordering would exhibit a clear signature in the real dielectric permittivity. Afterwards, both AC and DC conductivity can be determined by dielectric spectroscopy and henceforth enable simultaneous discussions on the conduction mechanism and the charge dynamics. The present study is performed along three crystallographic directions in order to treat the mechanism, as well as the dimensionality of the conduction.

II. EXPERIMENT

High-quality single crystals of $BaFe_2S_3$ and $BaFe_2Se_3$ were synthesized using a stoichiometric solid-state reaction method [14]. The sensitivity of the crystals to the growth conditions has already been established for these compounds. The impurity concentration in the sample affects its conduction, and pure samples tend to be more insulating [20]. Here, before the systematic study, we characterized several samples grown with different methods (self-flux vs Te flux [20,22,26] and grown in different crucibles, alumina vs carbon [5,6,10,14,22,26]). The samples with higher resistivity were the ones grown with self-flux method in carbon crucibles, which is also a desirable property for the dielectric measurements as it prevents effects of the electrode polarization; therefore those were chosen for our systematic study. For all specimens measured, the AFM transition temperatures were obtained via magnetic susceptibility measurements, yielding $T_N = 85$ and 178 K for $BaFe_2S_3$ and $BaFe_2Se_3$, respectively (see the Appendix).

Dielectric spectroscopy from 40 Hz to 10 MHz was performed with the help of an Agilent 4294A complex impedance analyzer. Utilizing a custom-made helium-flow cryostat the range from room temperature down to 5 K were covered. The electrical contacts were made with gold wires and carbon pastes using the standard pseudo-four-probe method [27]. Trying different contacts, carbon paste turned out to be the most suitable choice, as it reduces the spurious effects of the electrode polarization, due to the leakage currents from the sample. Measurements under magnetic field up to 9 T were performed inside an Oxford Spectromag superconducting magnet with a custom-made helium-flow cryostat.

The complex electrical impedance was measured as a function of temperature T and frequency f on $BaFe_2S_3$ and $BaFe_2Se_3$ to obtain the complex permittivity $\varepsilon^* = \varepsilon' + i\varepsilon''$, and the conductivity $\sigma_{AC}(f) = 2\pi f \varepsilon_0 \varepsilon''(f)$. The experiments have been performed on the same samples for $E \parallel a$, b, and c axes, after the contacts have been remade for the new crystallographic direction. The applied AC voltage was set to 0.05 V, assuring that the sample response stays in the ohmic regime throughout the measured temperature and frequency range; hence, the nonlinear effects can be discarded. The uncertainty in the measurements due to the determination of the geometrical factor is less than an order of magnitude between different directions.

III. RESULTS AND DISCUSSION

The theoretical prediction of ferroelectricity in this compound [24] motivated a previous dielectric study on $BaFe_2Se_3$ along the a axis (layer direction) [19]. A relaxor ferroelectric (RFE) behavior was identified right below T_N. However, owing to the strong electrode polarization effects that partially overlap with the observed RFE behavior, the origin of this signature could not be identified. Here we expanded the study to the other crystallographic directions and to the related compound $BaFe_2S_3$ to be able to identify the underlying mechanism. Moreover, the high-temperature electrode effects have been minimized by using carbon contacts; this way we can trace the relaxation behavior in a broader temperature and frequency range.

Figure 1 shows the temperature dependence of the real part of the permittivity $\varepsilon'(T)$ for $BaFe_2S_3$ and $BaFe_2Se_3$ along all the measured directions. First, our results confirm the absence of a strong ferroelectric signature, namely, a frequency-independent Curie-Weiss divergence at the transition temperature [28], as it was suggested for $BaFe_2Se_3$ along the rungs or layers. Instead, a RFE-like peak is observed in all

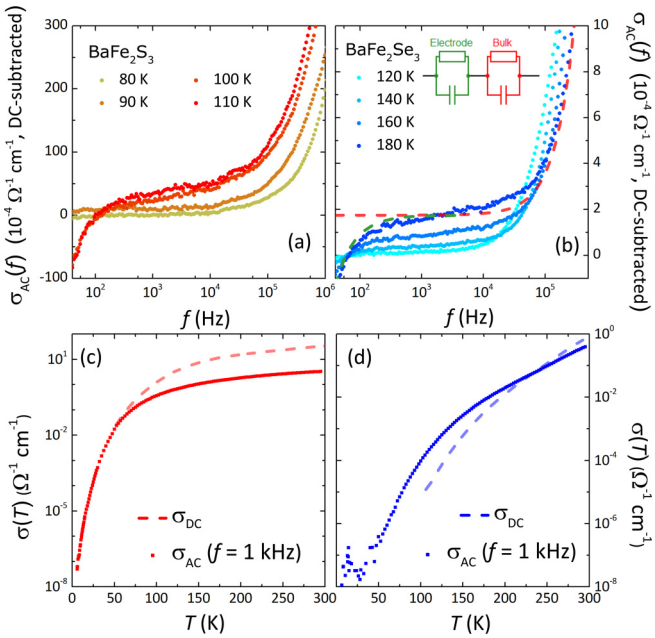

FIG. 2. (a) and (b) AC conductivity (with DC conductivity subtracted for clarity) along the leg direction in $BaFe_2S_3$ and $BaFe_2Se_3$, respectively. Dashed lines are bulk and electrode contributions interpreted from the equivalent circuit in the panel. (c) and (d) Temperature dependence of the DC conductivity obtained from DC resistivity measurements (dashed line) [14] and AC conductivity at $f = 1$ kHz (circles). The overlap of two curves indicates that the AC measurements level off to the DC values at low frequencies revealing the conduction in the samples.

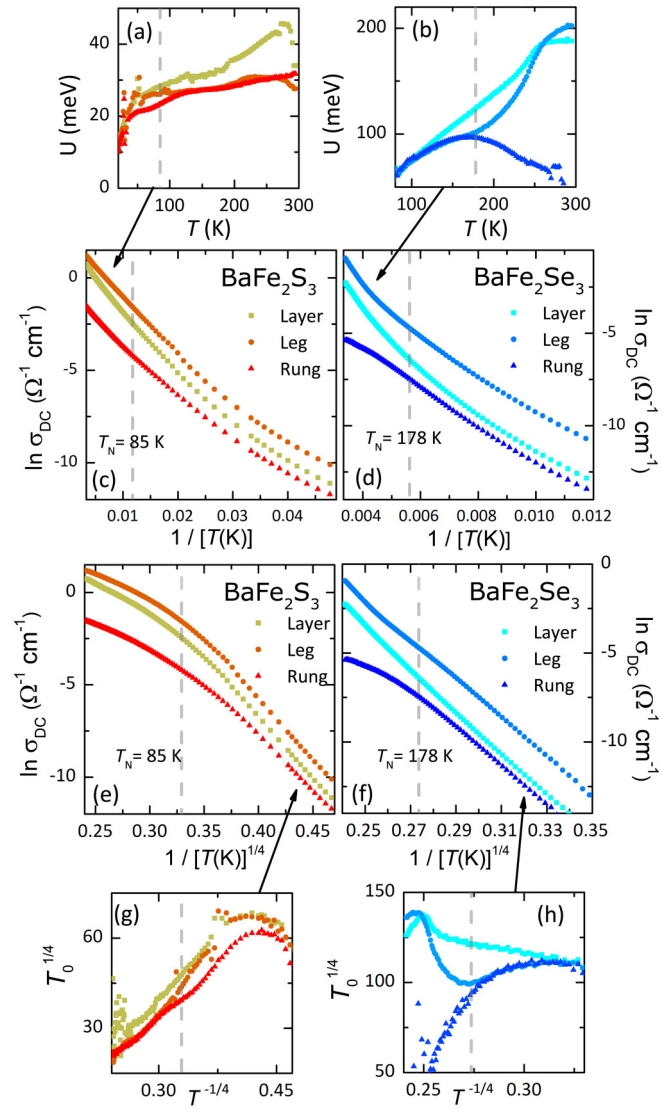

FIG. 3. Temperature dependence of the DC conductivity of $BaFe_2S_3$ and $BaFe_2Se_3$ for all polarizations plotted against (c) and (d) T^{-1} and (e) and (f) $T^{-1/4}$ to illustrate the behavior of Eqs. (1) and (2). Temperature evolutions of the fit parameter (a) and (b) U and (g) and (h) T_0 are plotted correspondingly. The gray dashed line in the plots indicates the AFM transition. Flat values of U (T_0) represents the sole correspondence of Eq. (1) [Eq. (2)] within the examined temperature range.

crystallographic directions for both $BaFe_2S_3$ and $BaFe_2Se_3$. RFE is mainly found in disordered solids or orientational glasses that contain nanoscale domains and thereby provide a distribution of relaxation times [29,30]. However, the observation of dispersive peaks in $\varepsilon'(T)$ cannot be taken as the decisive evidence for RFE. The relatively leaky nature of the samples and the dominant effect of electrodes, suggest that the observed relaxation dynamics is directly related to the conduction electrons in these systems; in principle this observation does not imply the effect of a dipolar reorientation. Therefore, we first examine the conductivity in these systems and clarify whether the observed relaxation behavior has the same origin.

Figures 2(a) and 2(b) depict the AC conductivities calculated from the imaginary part of the permittivity, $\sigma_{\mathrm{AC}}(f) = 2\pi f \varepsilon_0 \varepsilon''(f)$, in the temperature range below T_{N}. At high temperatures, the conductivity can be described with the low-frequency downturn due to the electrode polarization, which can be explained with the extrinsic Maxwell-Wagner effect due to the accumulation of space charges on the contacts [31]. However, the conductivity eventually levels off to a frequency-independent behavior indicating that the intrinsic effects are captured. This is further corroborated with the comparison of the AC and the DC conductivities. In Figs. 2(c) and 2(d) we plot the conductivity at $f \simeq 1$ kHz (solid line) together with the DC conductivity (dashed line) obtained from resistivity measurements [14]. The overlap of the two data indicates that $\sigma_{\mathrm{AC}}(f)$ levels off at 1 kHz allowing us to determine the intrinsic conduction in the system. Please note that, at low temperatures, the extrinsic effects are further shifted to the lower frequency range and out of our measurement window. The frequency-independent conductivity starts to increase with increasing f indicating the onset of another relaxation.

Usually, electronic transport in solids is conducted via nearest neighbor sites, which is well described by the Arrhenius equation:

$$\ln \sigma_{\mathrm{DC}} = -\frac{U}{k_B T} + \ln \sigma_0, \tag{1}$$

where U denotes the activation energy. If $\sigma(T)$ obeys the Arrhenius equation we can represent it as a straight line when

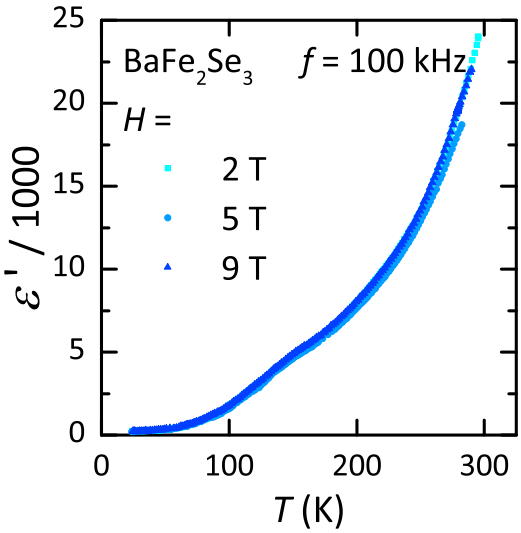

FIG. 4. Magnetodielectric permittivity in $BaFe_2Se_3$ at $H = 2$, 5, and 9 T with $E \parallel$ leg and $H \parallel$ layer.

plotted against T^{-1}. In Figs. 3(c) and 3(d) this behavior is found down to T_N but $\sigma(T)$ deviates from the straight line for $T < T_N$. Figures 3(a) and 3(b) depict the corresponding activation energy U in $BaFe_2S_3$ and $BaFe_2Se_3$ acquired from the fit by Eq. (1). At high temperature, $U \simeq 30$ and 200 meV for $BaFe_2S_3$ and $BaFe_2Se_3$, respectively. These values agree with the literature [13,14,19,22,23,32]. For both of the compounds, the obtained activation energies are similar along all crystallographic directions. Although the activated behavior at high temperatures is confirmed, the conduction exhibits a very anisotropic behavior, as expected from the highly anisotropic structure of the systems. In both compounds, conduction along the leg direction is significantly higher than along the layer or rung directions, as $\sigma_{\parallel \text{leg}}/\sigma_{\parallel \text{layer}} \simeq 2\,(\gtrsim 5)$ and $\sigma_{\parallel \text{leg}}/\sigma_{\parallel \text{rung}} \simeq 15\,(\gtrsim 15)$ for $BaFe_2S_3$ ($BaFe_2Se_3$). The clear change in slope below T_N cannot simply be explained with the change in activation energy due to magnetic order, as the scaling does not follow the Arrhenius behavior, anymore. The clear deviation from the Arrhenius law at low temperatures calls for another mechanism in these systems.

Besides the nearest neighbor activation, Mott's variable range hopping (VRH) is commonly reported as the dominant conduction mechanism in amorphous structures and often found in correlated electron systems, like organic charge-transfer salts [33–36]. VRH describes the phonon-assisted hopping of charge carriers exceeding the nearest neighbor localizations and predicts the following behavior [37]:

$$\ln \sigma_{\text{DC}} = -(T_0/T)^{1/(d+1)} + \ln \sigma_0, \tag{2}$$

where T_0 is the characteristic temperature related to the localization of states and its surrounding potential landscape, and the exponent is given by the dimensionality d of the conduction, i.e., isotropic three-, two-, and one-dimensional charge transport.

In Figs. 3(e) and 3(f) we plot $\sigma(T)$ for all axes of $BaFe_2S_3$ and $BaFe_2Se_3$ as a function of $T^{-1/4}$. Straight lines are found at $T < T_N$, indicating that 3D VRH is obeyed below the AFM ordering. Figures 3(g) and 3(h) show the temperature

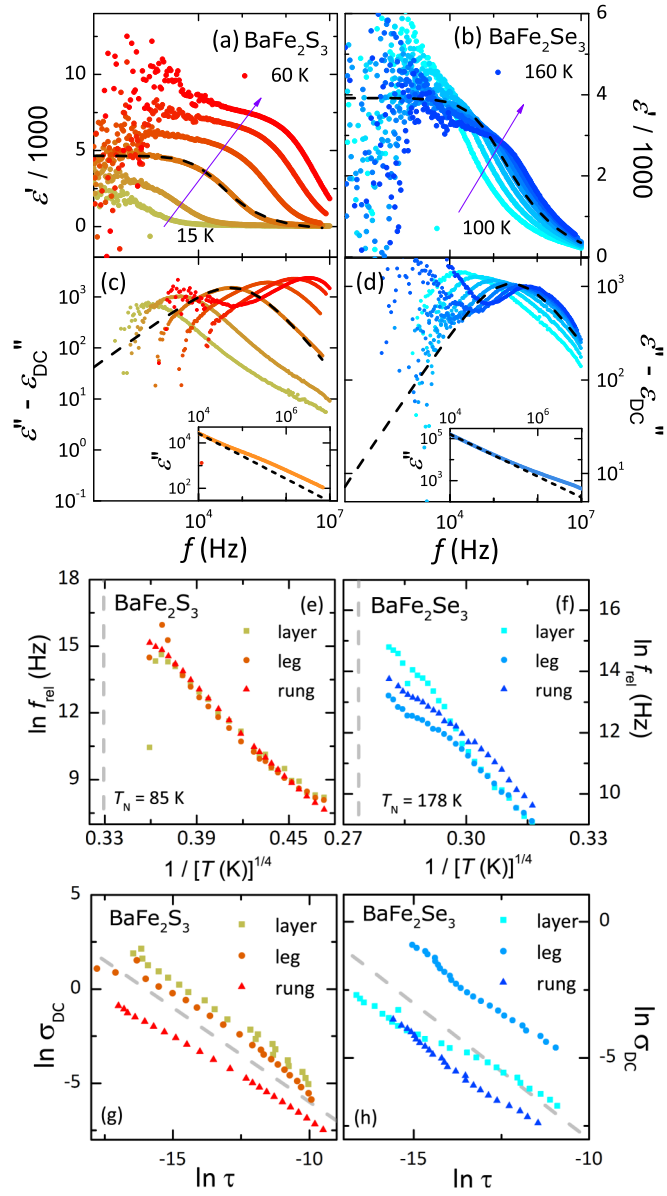

FIG. 5. Frequency dependence of the (a) and (b) real and (c) and (d) DC background subtracted imaginary permittivity in leg direction of $BaFe_2S_3$ and $BaFe_2Se_3$, respectively. Black dashed lines show the fits with Eq. (3). Inset: ε'' before subtraction of the DC contribution at $T = 30$ K (130 K) for $BaFe_2S_3$ ($BaFe_2Se_3$). Black short-dashed line illustrates the DC background. (e) and (f) Temperature dependence of the relaxation time obtained from the fits of Eq. (3). (g) and (h) Logarithmic plots of σ_{DC} against τ. The gray dashed line serves as a reference for slope -1.

evolution of T_0 and the levelling-off observed at low temperatures, indicating the crossover to the 3D VRH. In the intermediate temperature range, i.e., around T_N, a coexistence of two conduction mechanisms occurs with a gradual crossover. This gradual development of conduction resembles the development of the AFM ordering, suggesting the intimate relation of these two phenomena, as the transformation of magnetic phase also triggers the transformation of the charge transport mechanism. A similar change in the conduction mechanism triggered by magnetic order has been observed in

$LaTiO_3$ [38,39]. This switch in conduction can be attributed to the orbital fluctuations introduced by the AFM ordering. There is no significant magnetoconductivity [22] nor magnetodielectric permittivity (Fig. 4) in $BaFe_2Se_3$ under magnetic field up to 9 T. We explain this invariance by the robustness of the magnetic background of the system. T_N of a system indicates the strength of the local magnetization and it can give an estimate for the required magnetic field to perturb the system. With $T_N \simeq 180$ K, and with the relation $\mu_B H \approx k_B T$, we estimate that H is as high as $\simeq 260$ T, significantly higher than what our setup allows.

By combining the data from all three directions, we find that the charge carrier transport is governed by 3D hopping conduction in $BaFe_2Se_3$ (also in $BaFe_2S_3$), but the magnitudes of conductivity exhibit a huge anisotropy. The localization length α and average hopping distance l of the electrons are estimated from T_0 in VRH regime. $T_0 \simeq 1.7 \times 10^7$ and 1.5×10^8 for the sulfur and selenium compound. For 3D-VRH [33], $T_0 = 21.2/k_B g(E_F)\alpha^3$, where $g(E_F)$ is the density of state per volume, and $l \approx \alpha(T_0/T)^{1/4}$. In case of $BaFe_2S_3$ ($BaFe_2Se_3$), using lattice constants $a = 8.86(11.9)$ Å, $b = 11.3(5.41)$ Å, $c = 5.27(9.14)$ Å [1,16], and the values of $g(E_F) \simeq 8(15)\,\mathrm{eV}^{-1}$ [14], we obtain $\alpha \simeq 0.0976(0.0296)$ nm. The average hopping distance in $BaFe_2S_3$ and $BaFe_2Se_3$ vary from about 4.43 and 2.97 nm at low temperature to about 2.09 and 1.21 nm at T_N. This implies that the conductivity is confined to the smaller length scales when the unit cell doubles across the magnetic ordering.

Let us turn to the relaxations found in $\sigma_{AC}(f)$ at high frequencies in both compounds. Figures 5(a)–5(d) show the frequency dependence of the real and imaginary parts of the permittivity $\varepsilon^*(f)$, at the temperature where the relaxation was captured. Dielectric relaxation in solids can be described by the Havriliak-Negami equation [40]:

$$\varepsilon^* = \varepsilon_\infty + \frac{\varepsilon_s - \varepsilon_\infty}{[1 + (i\omega\tau)^{(1-\alpha)}]^\beta}, \tag{3}$$

where τ is the relaxation time, and α and β are characteristic parameters. The equation leads to a typical step and peak feature in $\varepsilon'(f)$ and $\varepsilon''(f)$, respectively. In the plots of $\varepsilon''(f)$, a DC background can be seen that overlaps with a clear relaxation peak. To better discuss the underlying relaxation process, we subtracted this DC contribution: the remaining $\varepsilon''(f)$ is plotted in Figs. 5(c) and 5(d) for both compounds. A distinct shift of the peak towards higher frequencies with increasing temperature is observed. Concomitantly, the shift of the steplike relaxation feature in $\varepsilon'(f)$ is present. In Figs. 5(e) and 5(f) the relaxation time is plotted as $\ln f_{rel}$ against $T^{-1/4}$. In none of the compounds, neither $BaFe_2S_3$ nor $BaFe_2Se_3$, do we see a noticeable anisotropy between polarizations, which is counterintuitive considering the quasi-1D structure. Similar to the evolution of $\sigma(T)$, $\ln f_{rel}$ from all polarizations in both $BaFe_2S_3$ and $BaFe_2Se_3$ behave linearly against $T^{-1/4}$ below T_N, suggesting the same origin for both the relaxation and the conduction. Combining these three observations: the agreement in temperature evolution with $\sigma(T)$, the isotropic nature of $\ln f_{rel}$, and the unusually high $\varepsilon'(T)$, it is more intuitive to attribute this relaxation process to itinerant charge carriers, instead of electric dipole dynamics.

Conductivity due to diffusive motions and dielectric relaxation of mobile charge carriers in solids is commonly modeled by the Debye-Stokes-Einstein equation [41,42], which suggests that σ_{DC} is inversely proportional to τ with a slope of unity. From Figs. 5(g) and 5(h) it becomes clear that the Debye-Stokes-Einstein equation is observed by both $BaFe_2S_3$ and $BaFe_2Se_3$; this confirms therefore that the relaxation at high frequency is the effect of mobile charge carriers instead of a reorientation of the dipoles.

IV. CONCLUSIONS

In a comparative study, the polarization dependence of the conductivity and permittivity of $BaFe_2S_3$ and $BaFe_2Se_3$ were thoroughly investigated. In both systems, a change in the conduction mechanism, from activated Arrhenius behavior to the variable range hopping is observed which is triggered by the antiferromagnetic ordering. The conductivity mechanism along all crystallographic directions shows a similar behavior, while the highly anisotropic nature of the systems is reflected in the absolute value of the conduction. In the hopping phase, i.e., below T_N, an isotropic relaxation is observed at MHz frequencies, which is attributed to the electronic polarization of mobile free charge carriers. No sign of ferroelectricity is observed in this study, but the possibility of realization remains as the dielectric response is overwhelmed by the free carriers. Finally, we would like to highlight the magnetic ordering influenced conduction, since it provides a microscopic picture to the interplay between magnetic and electronic structure in the iron-ladder series. On the other hand, the type of the magnetic order seems to have no affect on the observed conduction mechanism.

ACKNOWLEDGMENTS

The authors acknowledge the technical support from Gabriele Untereiner. The work in Korea was supported by the National Research Foundation (NRF) of Korea grant funded by the Korea Ministry of Science and ICT (No. 2012R1A3A2048816). E.U. acknowledges the European Social Fund and the Baden-Württemberg Stiftung for the financial support of this research project by the Eliteprogramme.

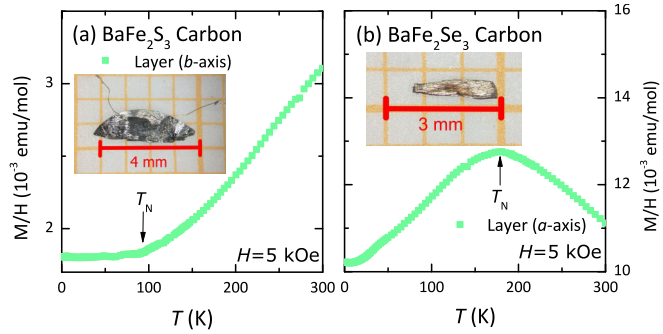

FIG. 6. Magnetic susceptibility measurements for (a) $BaFe_2S_3$ and (b) $BaFe_2Se_3$ synthesized in carbon crucibles along the layer direction with $H = 5$ kOe. The T_N are 85 and 178 K, respectively. Inset: Picture of the crystal.

APPENDIX: MAGNETIC SUSCEPTIBILITY MEASUREMENTS OF THE SAMPLES

Magnetic susceptibility of the specimens used in this study, $BaFe_2S_3$ and $BaFe_2Se_3$ synthesized in carbon crucibles, are depicted in Fig. 6. Magnetic field is applied along the layer direction with $H = 5$ kOe. The T_N are found to be 85 and 178 K for $BaFe_2S_3$ and $BaFe_2Se_3$, respectively.

[1] M. Mourigal, S. Wu, M. B. Stone, J. R. Neilson, J. M. Caron, T. M. McQueen, and C. L. Broholm, Block Magnetic Excitations in the Orbitally Selective Mott Insulator $BaFe_2Se_3$, Phys. Rev. Lett. **115**, 047401 (2015).

[2] Z. V. Popović, M. Šćepanović, N. Lazarević, M. Opačić, M. M. Radonjić, D. Tanasković, H. Lei, and C. Petrovic, Lattice dynamics of $BaFe_2X3$ (X = S, Se) compounds, Phys. Rev. B **91**, 064303 (2015).

[3] K. Takubo, Y. Yokoyama, H. Wadati, S. Iwasaki, T. Mizokawa, T. Boyko, R. Sutarto, F. He, K. Hashizume, S. Imaizumi, T. Aoyama, Y. Imai, and K. Ohgushi, Orbital order and fluctuations in the two-leg ladder materials $BaFe_2X_3$ (X=S and Se) and $CsFe_2Se_3$, Phys. Rev. B **96**, 115157 (2017).

[4] T. Yamauchi, Y. Hirata, Y. Ueda, and K. Ohgushi, Pressure-Induced Mott Transition Followed by a 24-K Superconducting Phase in $BaFe_2S_3$, Phys. Rev. Lett. **115**, 246402 (2015).

[5] H. Takahashi, A. Sugimoto, Y. Nambu, T. Yamauchi, Y. Hirata, T. Kawakami, M. Avdeev, K. Matsubayashi, F. Du, C. Kawashima, H. Soeda, S. Nakano, Y. Uwatoko, Y. Ueda, T. J. Sato, and K. Ohgushi, Pressure-induced superconductivity in the iron-based ladder material $BaFe_2S_3$, Nat. Mater. **14**, 1008 (2015).

[6] J. Ying, H. Lei, C. Petrovic, Y. Xiao, and V. V. Struzhkin, Interplay of magnetism and superconductivity in the compressed Fe-ladder compound $BaFe_2Se_3$, Phys. Rev. B **95**, 241109(R) (2017).

[7] Y. Zhang, L.-F. Lin, J.-J. Zhang, E. Dagotto, and S. Dong, Sequential structural and antiferromagnetic transitions in $BaFe_2Se_3$ under pressure, Phys. Rev. B **97**, 045119 (2018).

[8] H. Hosono, A. Yamamoto, H. Hiramatsu, and Y. Ma, Recent advances in iron-based superconductors toward applications, Mater. Today **21**, 278 (2018).

[9] V. Svitlyk, D. Chernyshov, E. Pomjakushina, A. Krzton-Maziopa, K. Conder, V. Pomjakushin, R. Pöttgen, and V. Dmitriev, Crystal structure of $BaFe_2Se_3$ as a function of temperature and pressure: Phase transition phenomena and high-order expansion of Landau potential, J. Phys.: Condens. Matter **25**, 315403 (2013).

[10] Y. Hirata, S. Maki, J.-i. Yamaura, T. Yamauchi, and K. Ohgushi, Effects of stoichiometry and substitution in quasi-one-dimensional iron chalcogenide $BaFe_2S_3$, Phys. Rev. B **92**, 205109 (2015).

[11] V. Svitlyk, G. Garbarino, A. D. Rosa, E. Pomjakushina, A. Krzton-Maziopa, K. Conder, M. Nunez-Regueiro, and M. Mezouar, High-pressure polymorphism of $BaFe_2Se_3$, J. Phys.: Condens. Matter **31**, 085401 (2019).

[12] Z. S. Gönen, P. Fournier, V. Smolyaninova, R. Greene, F. M. Araujo-Moreira, and B. Eichhorn, Magnetic and transport properties of $Ba_6Fe_8S_{15}$ and $BaFe_2S_3$: Magnetoresistance in a spin-glass-like Fe(II) system, Chem. Mater. **12**, 3331 (2000).

[13] Y. Nambu, K. Ohgushi, S. Suzuki, F. Du, M. Avdeev, Y. Uwatoko, K. Munakata, H. Fukazawa, S. Chi, Y. Ueda, and T. J. Sato, Block magnetism coupled with local distortion in the iron-based spin-ladder compound $BaFe_2Se_3$, Phys. Rev. B **85**, 064413 (2012).

[14] S. Roh, S. Shin, J. Jang, S. Lee, M. Lee, Y.-S. Seo, W. Li, T. Biesner, M. Dressel, J. Y. Rhee, T. Park, and J. Hwang, Magnetic-order-driven metal-insulator transitions in the quasi-one-dimensional spin-ladder compounds $BaFe_2S_3$ and $BaFe_2Se_3$, Phys. Rev. B **101**, 115118 (2020).

[15] J. Gao, Y. Teng, W. Liu, S. Chen, W. Tong, M. Li, X. Zhao, and X. Liu, The synthesis and magnetic properties of $BaFe_2Se_3$ single crystals, RSC Adv. **7**, 30433 (2017).

[16] S. Chi, Y. Uwatoko, H. Cao, Y. Hirata, K. Hashizume, T. Aoyama, and K. Ohgushi, Magnetic Precursor of the Pressure-Induced Superconductivity in Fe-ladder Compounds, Phys. Rev. Lett. **117**, 047003 (2016).

[17] A. Pratt, M. Kurahashi, X. Sun, D. Gilks, and Y. Yamauchi, Orbital-selective magnetism in the spin-ladder iron selenides $Ba_{1-x}K_xFe_2Se_3$, Phys. Rev. B **85**, 180409(R) (2012).

[18] T. Hawai, C. Kawashima, K. Ohgushi, K. Matsubayashi, Y. Nambu, Y. Uwatoko, T. J. Sato, and H. Takahashi, Pressure-induced metallization in iron-based ladder compounds $Ba_{1-x}Cs_xFe_2Se_3$, J. Phys. Soc. Jpn. **86**, 024701 (2017).

[19] X. Liu, C. Ma, C. Hou, Q. Chen, R. Sinclair, H. Zhou, Y. Yin, and X. Li, Structural, magnetic and dielectric properties of $BaFe_2Se_3$ crystals, Europhys. Lett. **126**, 27005 (2019).

[20] B. Saparov, S. Calder, B. Sipos, H. Cao, S. Chi, D. J. Singh, A. D. Christianson, M. D. Lumsden, and A. S. Sefat, Spin glass and semiconducting behavior in one-dimensional $BaFe_{2-\delta}Se_3(\delta \approx 0.2)$ crystals, Phys. Rev. B **84**, 245132 (2011).

[21] J. Herbrych, N. Kaushal, A. Nocera, G. Alvarez, A. Moreo, and E. Dagotto, Spin dynamics of the block orbital-selective Mott phase, Nat. Commun. **9**, 3736 (2018).

[22] H. Lei, H. Ryu, A. I. Frenkel, and C. Petrovic, Anisotropy in $BaFe_2Se_3$ single crystals with double chains of FeSe tetrahedra, Phys. Rev. B **84**, 214511 (2011).

[23] F. Du, Y. Hirata, K. Matsubayashi, Y. Uwatoko, Y. Ueda, and K. Ohgushi, Doping- and pressure-induced change of electrical and magnetic properties in the Fe-based spin-ladder compound $BaFe_2Se_3$, Phys. Rev. B **90**, 085143 (2014).

[24] S. Dong, J.-M. Liu, and E. Dagotto, $BaFe_2Se_3$: A High T_c Magnetic Multiferroic with Large Ferrielectric Polarization, Phys. Rev. Lett. **113**, 187204 (2014).

[25] T. Aoyama, S. Imaizumi, T. Togashi, Y. Sato, K. Hashizume, Y. Nambu, Y. Hirata, M. Matsubara, and K. Ohgushi, Polar state induced by block-type lattice distortions in $BaFe_2Se_3$ with quasi-one-dimensional ladder structure, Phys. Rev. B **99**, 241109(R) (2019).

[26] J. M. Caron, J. R. Neilson, D. C. Miller, A. Llobet, and T. M. McQueen, Iron displacements and magnetoelastic coupling in the antiferromagnetic spin-ladder compound $BaFe_2Se_3$, Phys. Rev. B **84**, 180409(R) (2011).

[27] Agilent 4294A Precision Impedance Analyzer Operation Manual, Keysight technologies, 7th ed. (2003).

[28] W. Heywang, K. Lubitz, and W. Wersing, *Piezoelectricity* (Springer, Berlin, 2008).

[29] L. E. Cross, Relaxor ferroelectrics, Ferroelectrics **76**, 241 (1987).

[30] W. Kleemann, Universal domain wall dynamics in disordered ferroic materials, Annu. Rev. Mater. Res. **37**, 415 (2007).

[31] P. Lunkenheimer and A. Loidl, Dielectric spectroscopy on organic charge-transfer salts, J. Phys.: Condens. Matter **27**, 373001 (2015).

[32] H. Lei, H. Ryu, V. Ivanovski, J. B. Warren, A. I. Frenkel, B. Cekic, W.-G. Yin, and C. Petrovic, Structure and physical properties of the layered iron oxychalcogenide $BaFe_2Se_2O$, Phys. Rev. B **86**, 195133 (2012).

[33] B. I. Shklovskii and A. L. Efros, *Electronic Properties of Doped Semiconductors* (Springer, Berlin, 1984).

[34] D. Yu, C. Wang, B. L. Wehrenberg, and P. Guyot-Sionnest, Variable Range Hopping Conduction in Semiconductor Nanocrystal Solids, Phys. Rev. Lett. **92**, 216802 (2004).

[35] B. Köhler, E. Rose, M. Dumm, G. Untereiner, and M. Dressel, Comprehensive transport study of anisotropy and ordering phenomena in quasi-one-dimensional $(TMTTF)_2X$ salts (X = PF_6, AsF_6, SbF_6, BF_4, ClO_4, ReO_4), Phys. Rev. B **84**, 035124 (2011).

[36] M. Pinterić, M. Čulo, O. Milat, M. Basletić, B. Korin-Hamzić, E. Tafra, A. Hamzić, T. Ivek, T. Peterseim, K. Miyagawa, K. Kanoda, J. A. Schlueter, M. Dressel, and S. Tomić, Anisotropic charge dynamics in the quantum spin-liquid candidate κ-$(BEDT\text{-}TTF)_2Cu_2(CN)_3$, Phys. Rev. B **90**, 195139 (2014).

[37] S. Elliott, A.c. conduction in amorphous chalcogenide and pnictide semiconductors, Adv. Phys. **36**, 135 (1987).

[38] J. Hemberger, H.-A. K. von Nidda, V. Fritsch, J. Deisenhofer, S. Lobina, T. Rudolf, P. Lunkenheimer, F. Lichtenberg, A. Loidl, D. Bruns, and B. Büchner, Evidence for Jahn-Teller Distortions at the Antiferromagnetic Transition in $LaTiO_3$, Phys. Rev. Lett. **91**, 066403 (2003).

[39] P. Lunkenheimer, T. Rudolf, J. Hemberger, A. Pimenov, S. Tachos, F. Lichtenberg, and A. Loidl, Dielectric properties and dynamical conductivity of $LaTiO_3$: From dc to optical frequencies, Phys. Rev. B **68**, 245108 (2003).

[40] K. Friedrich and S. Andreas, *Broadband Dielectric Spectroscopy* (Springer, Berlin, 2012).

[41] G. P. Johari and O. Andersson, On the nonlinear variation of dc conductivity with dielectric relaxation time, J. Chem. Phys. **125**, 124501 (2006).

[42] G. Power, J. K. Vij, and G. P. Johari, Structure-dependent dc conductivity and relaxation time in the Debye-Stokes-Einstein equation, J. Phys. Chem. B **111**, 11201 (2007).